An Overview of the Adaptive Robust DFT

Alexey A. Roenko, Vladimir V. Lukin, Igor Djurović

Abstract— **This paper overviews basic principles and applications of the robust-DFT (RDFT) approach, which is used for robust processing of frequency-modulated (FM) signals embedded in non-Gaussian heavy-tailed noise. In particular, we concentrate on the spectral analysis and filtering of signals corrupted by impulsive distortions using adaptive and non-adaptive robust estimators. Several adaptive estimators of location parameter are considered and it is shown that their application is preferable with respect to non-adaptive counterparts. This fact is demonstrated by efficiency comparison of adaptive and non-adaptive RDFT-methods for different noise environments.**

I. Introduction

Using Gaussian distributions, noise and other phenomena have been described over time in various applications such as communications, radars, sonars, acoustics, etc. [1]. However, recent studies have shown that heavier-tailed probability density functions (PDFs) provide a more adequate description of noise in many practical environments [2]-[4]. In particular, Spaulding and Middleton [2] initiated this development of various complex noise models. For example, variants of contaminated [5], generalized Gaussian distributions [6] and a family of symmetric α-stable (SαS) PDFs [3], [6] are models widely used to describe non-Gaussian noise environments. These realistic noise models have stimulated the development of robust estimators for nonlinear signal and image filtering [3], [5]-[7].

Theoretical developments behind linear filters have been concurrently performed in both temporal and spectral (Fourier transform) domains over the years [8]. Meanwhile, the theory of nonlinear filtering mainly focused on signal processing in the temporal domain. Typical robust filters include median, L-filters, α-trimmed mean filters [7], while recent contributions include more sophisticated filters such as FIR-hybrid median, weighted median and some other nonlinear filters [7]. Although classification and terminology used for linear filters can be hardly applied to nonlinear filters [9], they are generally regarded as low-pass filters and cannot be used as pass-band, stop-band and/or high-pass filters. Arce and his coworkers recently introduced a class of weighted median and myriad filters admitting negative weights [9]-[11]. These filters can be used to design nonlinear filters of all types (low-pass, high-pass, stop-band, and band-pass), while simultaneously removing impulsive noise. This development has renewed interests for the design and analysis of robust filters [12].

Practically at the same time, an alternative way to cope with non-Gaussian noise has been proposed by Katkovnik [13]. His contribution was followed by several other papers [14]-[17] where various robust periodogram and DFT forms were proposed. In particular, these so-called robust DFT (RDFT) methods estimate real (RE) and imaginary (IM) components of signal Fourier spectrum in a robust manner. The standard set of the robust estimators can be used for this task including M, L, and R-estimators [5]. In addition, the adaptive RDFT-forms have been proposed as well [14]-[20]. These transform are further generalized in various application including the time-frequency analysis [21], [22], radars [23], [24], filtering of frequency-modulated (FM) and pulse-like signals [20], [25] and the estimation of signal parameters [21], [26].

The goal of this paper is to analyze and recommend proper RDFT forms for various signal-noise scenarios. Therefore, the paper is organized as follows: we discuss design chal-

EURASIP Journal on Advances in Signal Processing, special issue "Robust Processing of Nonstationary Signals", Vol. 2010, Article ID 595071, 2010.

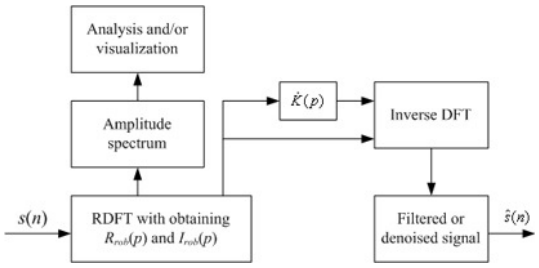

Fig. 1. Block diagram for signal processing approach based on RDFT

lenges in Section 2, while various adaptive and non-adaptive robust estimators are described in Section 3. The results of a numerical analysis of non-adaptive and adaptive RDFT-methods are covered in Section 4.

II. RDFT framework and requirements to robust estimators

Consider a one-dimensional (1D) discrete signal $s(n)$ corrupted by non-Gaussian noise $\nu(n)$

$$x(n) = s(n) + \nu(n) \tag{1}$$

where $n\in[1,N]$. To filter $x(n)$ using the RDFT-based approach we implement the following steps [13], [14], [16]-[20]:

1. Calculate the RDFT for the analyzed signal;
2. Multiply the obtained spectrum estimate, $\dot{X}_{rob}(p)$ ($p\in[0,N\text{-}1]$ is the frequency index), with specified frequency characteristic ;
3. Calculate the standard inverse DFT.

The block diagram of the RDFT-based signal processing approach is shown in Fig. 1. The RDFT can be used in all applications where the standard DFT is commonly applied. For example, the RDFT is used for the time-frequency analysis in [27].

The complex-valued spectrum obtained by RDFT-method can be written as

$$\dot{X}_{rob}(p) = R_{rob}(p) + jI_{rob}(p) \tag{2}$$

where $R_{rob}(p)$ and $I_{rob}(p)$ are the robust estimates of RE and IM components of the DFT. The index p corresponds to frequencies f_p as $f_p=p\Delta f$, $\Delta f=1/NT_S$; $R_{rob}(p)=R_{rob}(f_p)$, $I_{rob}(p)=I_{rob}(f_p)$, where T_S represents the sampling period.

The optimal DFT method for Gaussian noise averages $x(n)\exp(\text{-}j2\pi f_p nT_S)=x(n)\exp(\text{-}j2\pi pn/N)$ for each frequency (i.e., the standard DFT):

$$\begin{aligned}\dot{X}_S(p) &= \dot{X}_S(f_p) = \\ &= \frac{1}{N}\sum_{n=1}^{N} x(n)\exp\left(-j2\pi pn/N\right) \\ &= \text{mean}\left\{\text{x(n)}\exp\left(-\text{j}2\pi\text{pn/N}\right)\right\} = \\ &= \text{mean}\left\{\text{Re}\left[\text{x(n)}\exp\left(-\text{j}2\pi\text{pn/N}\right)\right]\right\} \\ &+j\text{mean}\left\{\text{Im}\left[\text{x(n)}\exp\left(-\text{j}2\pi\text{pn/N}\right)\right]\right\}\end{aligned} \tag{3}$$

where Re and Im denote real and imaginary parts of a complex-valued number. Generally, the RDFT can be described as:

$$\begin{aligned}R_{rob}(p) &= T\left\{Re\left[x(n)\exp\left(-j2\pi pn/N\right)\right]\right\}, \\ I_{rob}(p) &= T\left\{Im\left[x(n)\exp\left(-j2\pi pn/N\right)\right]\right\}\end{aligned} \tag{4}$$

where $T\{\cdot\}$ denotes applied robust estimator. It should be mentioned that there are many different robust estimators. Hence, such an estimator, $T\{\cdot\}$, should be carefully chosen since the resulting properties of the corresponding RDFT-methods depend on $T\{\cdot\}$.

The RDFT-based signal processing methods should provide accurate results in the following cases:

1. A signal, $s(n)$, can be either "smooth" or "high-frequency" (note that in the latter case the standard low-pass nonlinear filters cause signal degradation [9]).
2. Noise can resemble the Gaussian case or it might have heavy-tailed PDF [28]. Furthermore, limited a priori information about noise statistics may exist, but not necessarily.

By applying the robust operators in (4), we obtain significant improvements in comparison to the mean-operators for heavy-tailed noise environments [13], [14]. The presence of only one or a few samples corrupted by impulse(s) can lead to considerable deterioration of $\dot{X}_S(p)$. The RDFT methods suppress these outliers and achieve more accurate estimates of the non-noisy signal spectrum. Therefore, the major task is to obtain $\dot{X}_{rob}(p)=R_{rob}(p)+jI_{rob}(p)$ as close to

$$\dot{S}(p) = \text{mean}\left\{\text{Re}\left[\text{s(n)}\exp\left(-\text{j}2\pi\text{pn/N}\right)\right]\right\}$$

$$+j\text{mean}\{\text{Im}[\text{s(n)}\exp(-\text{j}2\pi\text{pn/N})]\} = \\ = R_S(p) + jI_S(p) \quad (5)$$

as possible for each f_p.

However, it is not an easy task. To illustrate this problem consider a simple case of a real-valued harmonic signal $s_1(n)=s_1(nT_S)=A\sin(2\pi FnT_S)$ where F=50 Hz, A=5, corrupted by zero-mean Gaussian noise $\nu(n)$. Fig. 2 represents the amplitude spectrum obtained by the standard DFT and its estimates $\left|\dot{S}_{\text{MED}}(p)\right|$, $R_{MED}(p)$ and $I_{MED}(p)$ evaluated by the RDFT-method, where $T\{...\}$ is the sample median (MED). It can be clearly seen that the estimate $\left|\dot{S}_{\text{MED}}(p)\right|$ differs from the conventional spectrum due to distortions introduced in $I_{MED}(p)$ (for a test signal $A\cos(2\pi FnT_S)$ distortions appear in $R_{MED}(p)$). To further understand the appearance of these undesirable disturbances, we consider the histograms of the samples $R(p,n)=\{x(n)\cos(2\pi pn/N)\}$ and $I(p,n)=\{\text{-}x(n)\sin(2\pi pn/N)\}$ for two frequencies: $f_p=F$ where there are no distortions introduced by RDFT-method, and $f_p=3F=150$ Hz where is considerably distorted (see Fig. 2b). Values of the corresponding estimators $R_S(p)$, $I_S(p)$, $R_{MED}(p)$ and $I_{MED}(p)$ are marked at histograms by solid and dashed lines, respectively. For each histogram we have determined the percentile coefficient of kurtosis (PCK) [29] (for mathematical definition see Appendix 1). This parameter characterizes the distribution tail heaviness. For Gaussian PDF it is equal to 0.26 while for distributions with heavier tails PCK is smaller. For SαS processes, the PCK value decreases when α value becomes smaller.

In parallel, the median of absolute deviations (MAD) from the sample median has been calculated to characterize the data scale (see Appendix 1). MAD is used instead of the standard deviation since considered distributions might have heavy tails. This will be demonstrated later.

Let us analyze the histograms for $f_p=F$ shown in Fig. 3a, b. Both represented histograms are symmetric with respect to their location parameter (LP). Then, $R_{MED}(p)=R_S(p)$ and $I_{MED}(p)=I_S(p)$. Consider the second case with $f_p=3F$. The corresponding histograms represented in Figs. 3c and d show that the $R(p,n)$ distribution is again symmetric with respect to its LP, whereas the histogram of $I(p,n)$ is asymmetric. Then $I_S(p)$ and $I_{MED}(p)$ differ as in the cases of other asymmetric PDFs like Rayleigh distribution [30]. Contrary to the previous case, the values of PCK and MAD are also different for PDFs of RE and IM components.

The fact that $I_{MED}(p)?I_S(p)$ for some frequencies introduces distortions in a signal spectrum estimate. Then, the spectrum estimate distortions lead to the distortions of the filtered signal in temporal domain. Recall that the filtered signal is obtained by using the inverse standard DFT of the robust estimate $\dot{S}_{rob}(p)$.

Aforementioned problem is common for some other robust estimators. For example, if one uses α-trimmed mean estimator (ATM), distortions in the output (filtered) signal are observed as well. They are clearly demonstrated in Fig. 4. This spectral distortion effect is undesirable and the main goal is its minimization in the RDFT-based signal processing methods.

Now consider the case of a signal corrupted by Gaussian noise for two different values of the standard deviation, σ_G=1 and σ_G=10. The histograms for two frequencies $f_p=F$ and $f_p=3F$ for σ_G=1 are presented in Figs. 5a-d. As it can be seen the distributions in Figs. 5a, b are light-tailed but not symmetric; $R_{MED}(p)?R_S(p)$, $I_{MED}(p)?I_S(p)$. The PDFs depicted in Fig. 5c, d, are also asymmetric but with heavier tails. Distribution scales are in both cases approximately the same.

The histograms for $f_p=F$ and $f_p=3F$ for σ_G=10 are presented in Figs. 5e-h, respectively. MAD values have considerably increased in comparison to previous cases (σ_G=1). All distributions are almost symmetric and they have heavy tails. Thus, the presence of input noise has considerably changed PDF properties of the considered data samples in comparison to the earlier considered case of noise absence. Since the distributions are heavy-tailed, the use of robust estimators can

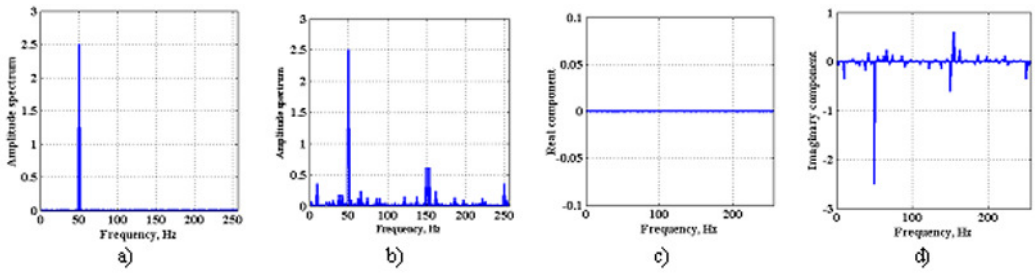

Fig. 2. Amplitude spectrum estimates of noise-free signal $s_1(n)$ obtained by standard DFT (a) and RDFT-method based on MED (b); $R_{MED}(p)$ (c) and $I_{MED}(p)$ (d)

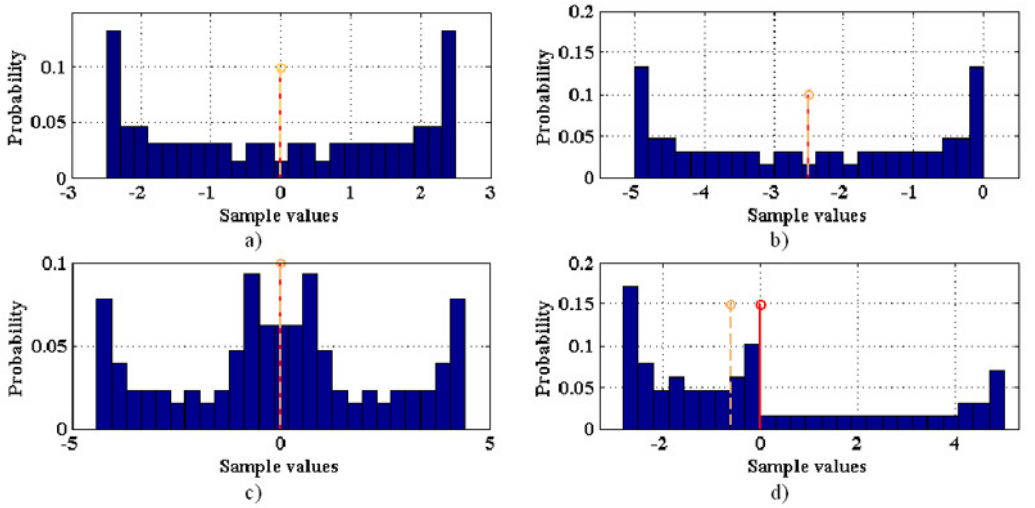

Fig. 3. Histograms of $R(p,n)$ (left column) and $I(p,n)$ (right column) for f_p=F (a and b) PCK_{RE}=PCK_{IM}=0.37, MAD_{RE}=MAD_{IM}=1.77 (a and b); for f_p=$3F$ (c and d) PCK_{RE}=0.19, MAD_{RE}=1.47 (c), PCK_{IM}=0.28, MAD_{IM}=1.71 (d)

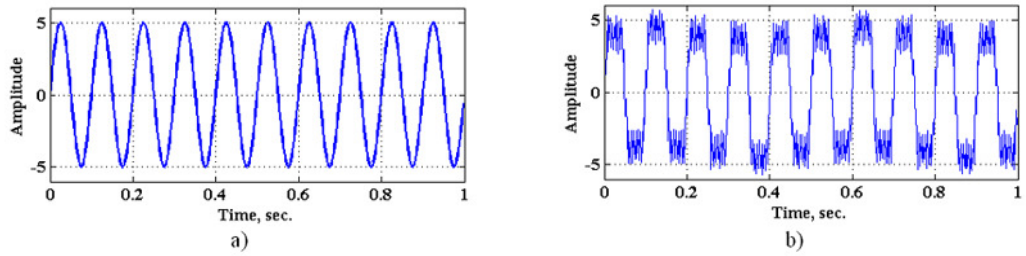

Fig. 4. Example of distortions introduced by ATM-method of RDFT: the noise-free harmonic signal (F=10 Hz) (a) and its estimate obtained using inverse DFT of $\dot{S}_{\mathrm{ATM}}(p)$ (b)

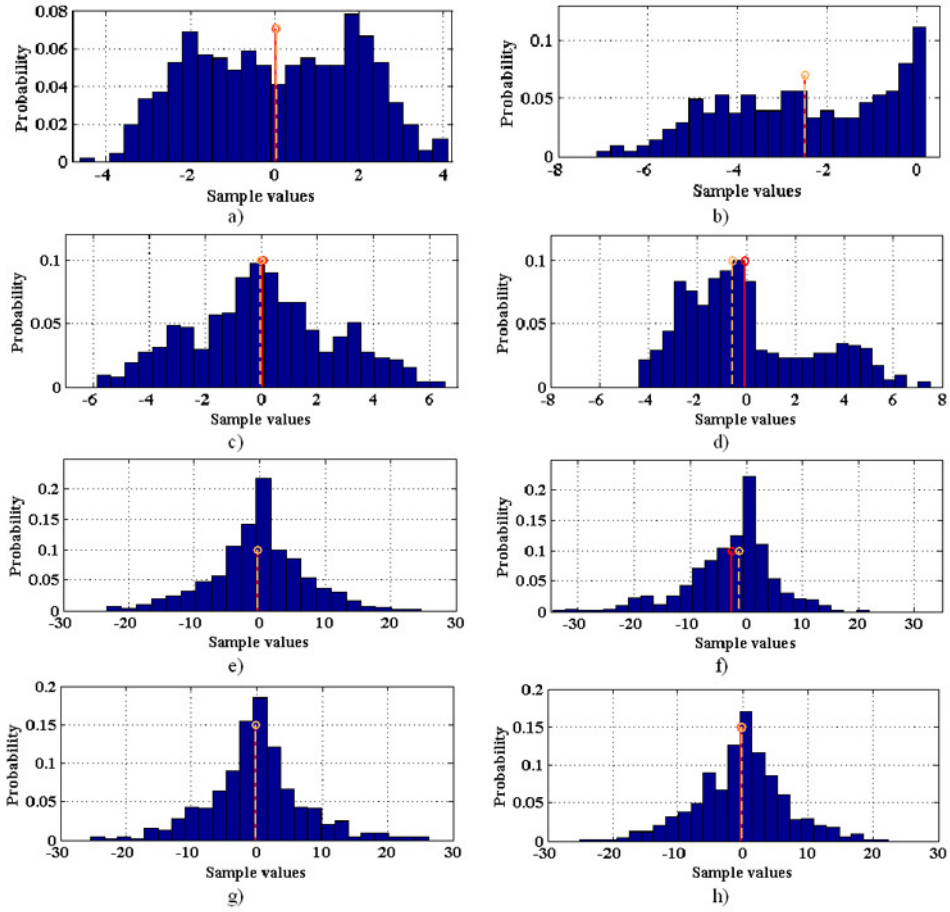

Fig. 5. Histograms of $R(p,n)$ (left column) and $I(p,n)$ (right column) for:
- f_p=F, σ_G=1; PCK$_{RE}$=0.330, MAD$_{RE}$=1.65, PCK$_{IM}$=0.341, MAD$_{IM}$=1.73 (a and b)
- f_p=3F, σ_G=1; PCK$_{RE}$=0.243, MAD$_{RE}$=1.67, PCK$_{IM}$=0.252, MAD$_{IM}$=1.68 (c and d)
- f_p=F, σ_G=10; PCK$_{RE}$=0.209, MAD$_{RE}$=3.77, PCK$_{IM}$=0.231, MAD$_{IM}$=3.94 (e and f)
- f_p=3F, σ_G=10; PCK$_{RE}$=0.186, MAD$_{RE}$=3.46, PCK$_{IM}$=0.237, MAD$_{IM}$=3.92 (g and h)

give us some benefits.

Now, we analyze the accuracy of the RDFT-methods and compare with the standard DFT. The MSE of the spectrum estimate is calculated as:

$$\mathrm{MSE_i} = \frac{1}{\mathrm{M}} \sum_{\mathrm{m=1}}^{\mathrm{M}} \mathrm{MSE_i(m)}, \tag{6}$$

$$\mathrm{MSE_i\,(m)} = \frac{1}{\mathrm{N}} \sum_{\mathrm{p=0}}^{\mathrm{N-1}} \left| \dot{\mathrm{X}}_{\mathrm{i}}^{\mathrm{m}}(\mathrm{p}) - \dot{\mathrm{S}}(\mathrm{p}) \right|^2, \tag{7}$$

where $\dot{X}_i^m(p)$ is the estimate of the spectrum obtained by the i-th method for the m-th signal realization; i denotes the investigated method where the standard DFT and the RDFT-method based on MED are considered; M=100 is the number of realizations.

The results are presented in Table 1. As expected, the MSE for the standard DFT (MSE$_{ST}$) increases proportionally to σ_G^2. For RDFT-method based on MED, MSE$_{MED}$ is not equal to zero even for σ_G=0. This is due to the previously described distortions. However, for large σ_G (see, for instance, σ_G=4), the value of MSE$_{MED}$ is considerably smaller than MSE$_{ST}$, i.e., the median RDFT-form gives better estimation of the DFT. Thus, advan-

tages of the RDFT based processing become apparent for rather important practical case of low input SNR even for the Gaussian input noise.

Next, consider another marginal case where the input sample is equal to noise without signal. This scenario is particularly important when dealing with signal detection where it is desirable to decrease noise level at the output.

Fig. 6 represents a realization of heavy-tailed noise (modeled as a product of two independent zero-mean white Gaussian variables with σ_G=1) and its estimate obtained as the inverse DFT of $\dot{X}_{\mathrm{MED}}(p)$. Clearly, impulses have been removed and noise has become less intensive. Here, we would like to emphasize that the distribution of modulated noise $\nu(n)\sin(2\pi f_p T_S n/N)$ is not equal to the distribution of $\nu(n)$ [31].

Consider now a more complicated case of a FM-signal. As a case study, let us analyze signal $s_2(n)$=$A\sin(2\pi F(n) n T_S)$ where A=5, $F(n)$=anT_S, for n=0 F=0, for nT_S=1 sec., F=50 Hz (a=50). Figs. 7a-c represent , $R_S(p)$ and $I_S(p)$ for the considered noise-free signal. There is a range of frequencies (over 100 Hz) for which , $R_S(p)$ and $I_S(p)$ are practically equal to zero. The estimates $\left|\dot{S}_{\mathrm{MED}}(p)\right|$, R_{MED} (p) and I_{MED} (p), evaluated by RDFT-method based on the MED, are demonstrated in Figs. 7d-f. Again, the RDFT-method introduces distortions.

Consider the histograms of $R(p,n)$ and $I(p,n)$ for two frequencies. Let us first analyze the histograms for the frequency f_p=32 Hz which is inside the signal spectrum band. Just for this frequency the spectrum distortions are quite large. As demonstrated in Figs. 8a-b, we obtain asymmetric distributions, inducing a lack of overlap between the mean and MED values. Note that these distributions for the FM signal $s_2(n)$ considerably differ from those ones for the harmonic signal $s_1(n)$ shown in Fig. 3.

Next, let us analyze the case when Gaussian noise is present. Histograms for f_p=32 Hz are shown in Figs. 8c,d (σ_G =10). The distributions have become heavy-tailed with wider limits in comparison to the distributions shown in Figs. 8a,b. The obtained MSEs of spectrum estimates for noise-free and noisy signal $s_2(n)$ are presented in Table 2. For the standard DFT, the MSE increases proportionally to σ_G as in the previous case. For the MED-method of RDFT, MSE_{MED} is not equal to zero even for σ_G=0 due to introduced distortions. For large σ_G (for example, σ_G =10), the MSE_{MED} value is almost four times smaller than the MSE_{ST} value, i.e., the RDFT approach achieves a more accurate estimate of the spectrum for low values of the input SNR.

Concluding the analysis, we can state the following: first, there are practical cases when even the simplest RDFT|method yields more accurate results than the standard DFT. However, there are also cases when RDFT introduces considerable distortions. Taking into account the abovementioned properties, the spectrum estimate obtained by RDFT-methods can be represented as

$$\widehat{\dot{X}}(p) = \widehat{R}(p) + j\widehat{I}(p)$$
$$= [R_s(p) + \triangle\, R(p)] + j\,[I_s(p) + \triangle\, I(p)] \quad (8)$$

where the requirement for estimators is to provide

$$|\triangle \mathrm{R(p)}| \to \min,\ |\triangle \mathrm{I(p)}| \to \min \quad (9)$$

for each p. Note that if (9) is satisfied, noise is suppressed in the temporal domain after the inverse DFT. Therefore, we analyze the estimators meeting these criteria in Section 3.

III. Adaptive robust estimators and their properties

There is a profound theory of LP estimation for data samples with symmetric distributions [5], [29]. It allows obtaining optimal maximum-likelihood (ML) and L-estimators for data realizations with a priori known PDFs. However, distributions of modulated signal samples for each considered frequency in RDFT data processing approach are unknown in advance.

There are also methods for robust mode finding based on adaptive myriad or interquantile estimators [31], [32]. However, $R_S(p)$

TABLE I
MSE FOR SIGNAL $s_1(n)$ SPECTRUM ESTIMATES OBTAINED BY STANDARD DFT AND RDFT-METHOD BASED ON MED FOR THE CASE OF GAUSSIAN NOISE WITH DIFFERENT VALUES OF σ_G

	σ_G						
	0	0.5	1	2	4	8	10
MSE_{ST}	0	0.0005	0.0020	0.0078	0.0313	0.1240	0.1949
MSE_{MED}	0.0055	0.0052	0.0052	0.0061	0.0123	0.0350	0.0547

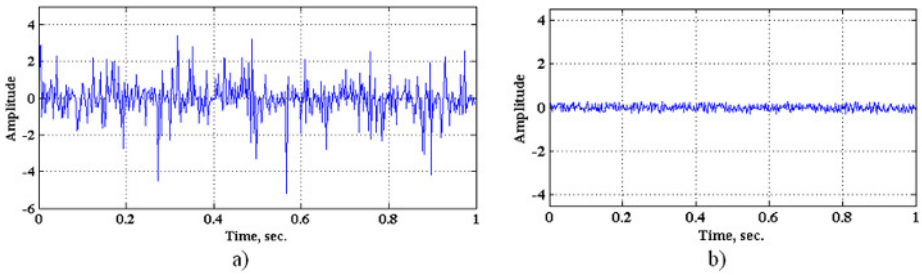

Fig. 6. The realization of the original heavy-tailed noise (σ_G=1) and its estimate obtained after inverse DFT of $\dot{X}_{\text{MED}}(p)$

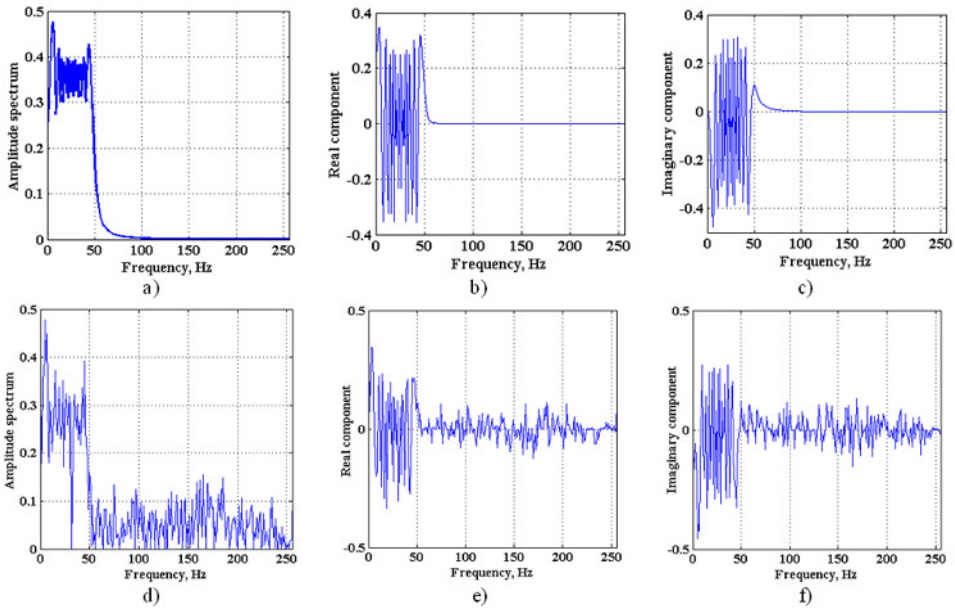

Fig. 7. Amplitude spectrum of noise-free FM signal $s_2(n)$ (left column), and its RE (central column) and IM (right column) components obtained by standard DFT (a-c) and MED-form of RDFT (d-f)

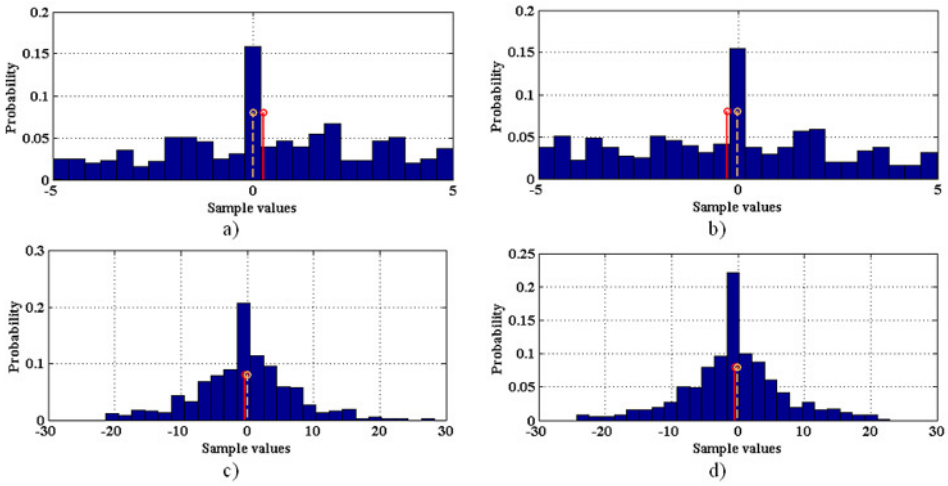

Fig. 8. Histograms of $R(p,n)$ (left column) and $I(p,n)$ (right column) for noise-free (a and b) and noisy (c and d) FM-signal $s_2(n)$ for f_p=32 Hz; PCK_{RE}=0.250, MAD_{RE}=1.838, PCK_{IM}=0.261, MAD_{IM}=1.84 (noise-free case)
PCK_{RE}=0.219, MAD_{RE}=3.75, PCK_{IM}=0.211, MAD_{IM}=3.74 (noisy case)

TABLE II
MSE FOR SIGNAL $s_2(n)$ SPECTRUM ESTIMATES OBTAINED BY STANDARD DFT AND RDFT-METHOD BASED ON MED FOR THE CASE OF GAUSSIAN NOISE WITH DIFFERENT VALUES OF σ_G

	σ_G						
	0	0.5	1	2	4	8	10
MSE_{ST}	0	0.00039	0.00163	0.00671	0.0270	0.1077	0.1725
MSE_{MED}	0.00543	0.00555	0.00610	0.00845	0.0154	0.0317	0.0459

and $I_S(p)$ can be considerably different from modes of the corresponding distributions (see examples in Fig. 5). There are also other adaptive estimators, e.g., [33], that are mainly intended on processing data samples with heavy-tailed PDFs.

In Section 2, we analyzed histograms $R(p,n)$ and $I(p,n)$ for particular frequencies. To gain further understanding of the desirable properties of the RDFT estimators we analyze scale and tail heaviness for these data samples for all spectral frequencies of FM signal $s_2(n)$ corrupted by non-Gaussian noise (Fig. 9). As a practical example, consider noise modeled as the SαS process with α=1.5 and γ=1. Note that such a value of α is typical for atmospheric noise [33]. As it is seen in Fig. 9b, the signal is corrupted with several impulses.

The plots of $\mathrm{MAD}_{RE}(p)$, $\mathrm{MAD}_{IM}(p)$, $\mathrm{PCK}_{RE}(p)$ and $\mathrm{PCK}_{IM}(p)$ for α=1.5 and γ=1 are given in Fig. 10. Each value of PCK and MAD obtained for each p-th frequency is averaged over 10 realizations to get more consistent values. Practically for all frequencies (except the 256-th), $\mathrm{MAD}_{RE}(p)$ and $\mathrm{MAD}_{IM}(p)$ are approximately equal. The values of $\mathrm{PCK}_{RE}(p)$ and $\mathrm{PCK}_{IM}(p)$ (except p=$N/2$=256) are approximately equal as well. They do not significantly differ from value 0.267 typical for a Gaussian PDF. This indicates that the distribution for all these frequencies is approximately equal to Gaussian.

A special case is the distributions for the p=$N/4$ which equals to f_p=128 Hz for the considered example. Both MAD and PCK are close to zero in this case. The reason is that for this frequency there are many values of $x(n)\cos(2\pi pn/N)$ and $x(n)\sin(2\pi pn/N)$ that are equal to zero. If p=$N/4$ then $2\pi Nn/4N$=$\pi n/2$ and for each odd n the val-

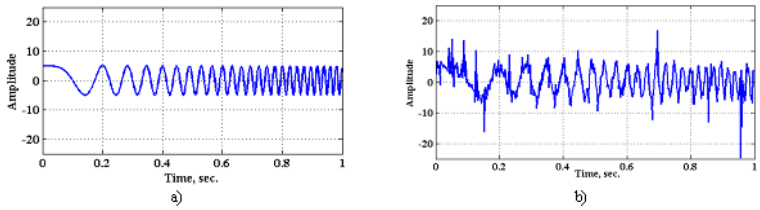

Fig. 9. The test noise-free FM signal $s_2(n)$ (a) and its realization corrupted by SαS noise with α=1.5 and γ=1 (b)

ues of $\cos(2\pi pn/N)$ are equal to 0. The same holds for all even n for $\sin(2\pi pn/N)$.

Now consider the case when α=1.5 and γ=4, i.e., stronger intensity noise. The plots of $\mathrm{MAD}_{RE}(p)$, $\mathrm{MAD}_{IM}(p)$, $\mathrm{PCK}_{RE}(p)$ and $\mathrm{PCK}_{IM}(p)$ are given in Fig. 11. For all frequencies (except the 256-th), $\mathrm{MAD}_{RE}(p)$, $\mathrm{MAD}_{IM}(p)$ are approximately equal, but they have slightly increased in comparison to those presented in Fig. 10. The values $\mathrm{PCK}_{RE}(p)$ and $\mathrm{PCK}_{IM}(p)$ (except p=$N/2$=256) are approximately equal, but have decreased compared to Fig. 10. They are now approximately equal to 0.2, i.e. the PDF sufficiently differs from the Gaussian distribution and has heavy tails. This implies that even when noise tail heaviness is known in advance, the characteristics of noise in $R(p,n)$ and $I(p,n)$ described by $\mathrm{PCK}_{RE}(p)$ and $\mathrm{PCK}_{IM}(p)$ can vary depending upon SNR. Then, one has to adapt to distribution characteristics of $R(p,n)$ and $I(p,n)$ in order to provide accurate spectral estimation and denoising.

As it follows from the analysis, the estimator should be robust to outliers but also close to the sample mean for PDFs without heavy tails (see Fig. 3 and 5).

Two examples of such estimators are Wilcoxon (WE) and Hodges-Lehmann (HL) estimators [34], [35] (for details see Appendix 1). Their statistical properties are quite similar, but the latter one requires less computations especially for a large sample size N. Therefore, we consider the HL estimator below. Note that these robust estimators produce the LP estimates close to the sample mean [36] for the Gaussian PDF.

Another estimator obeying the desired property is the ATM [5], [7], [29] with the trimming parameter β=N_β/N where N_β defines the number of outer trimmed elements for a data sample of size N (see Appendix 1). A well-known property of ATM is to be equal to the MED if β?0.5 and to the sample mean if β?0 [7].

A third estimator capable of producing an estimate close to the mean for non-noisy signals is the sample myriad (MYR) under the condition that its tunable parameter K is considerably larger than the standard deviation of the data sample [37]. In practice, it is sufficient to set K greater than the data sample standard deviation multiplied by 3 [38], [39]. The definition of the MYR is represented in Appendix 1. Main properties of the MYR estimator can significantly vary depending on the value of K. In particular, for a relatively small K, MYR is able to perform as an efficient mode finder for both symmetric and asymmetric distributions [6], [30].

Therefore, we conclude that there are several robust estimators which under certain conditions are capable of producing a desired behavior for data samples. However, for modulated signal samples we have different statistics for $R(p,n)$ and $I(p,n)$ for each frequency (see Figs. 5 and 8). Then, a question is how an estimator can adapt to such situations of a priori unknown or changing properties of underlying distributions? Obviously, we need some sort of adaptive RDFT estimators.

One of these solutions is the Taguchi's adaptive alpha-trimmed mean estimator (AATME) [40]. A second solution [17] is the adaptive estimator that presumes simple hard switching (AD HS) between the MED (applied if an estimated PCK for a data sample is smaller than

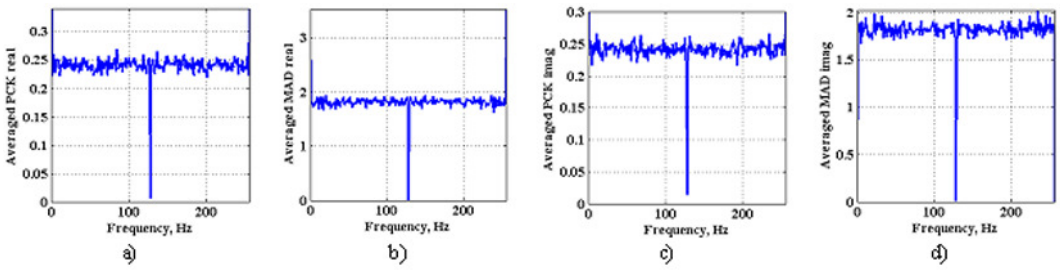

Fig. 10. The plots of $\mathrm{PCK}_{RE}(p)$ (a) and $\mathrm{PCK}_{IM}(p)$ (c), $\mathrm{MAD}_{RE}(p)$ (b) and $\mathrm{MAD}_{IM}(p)$ (d) for FM signal $s_2(n)$ corrupted by SαS noise with α=1.5 and γ=1

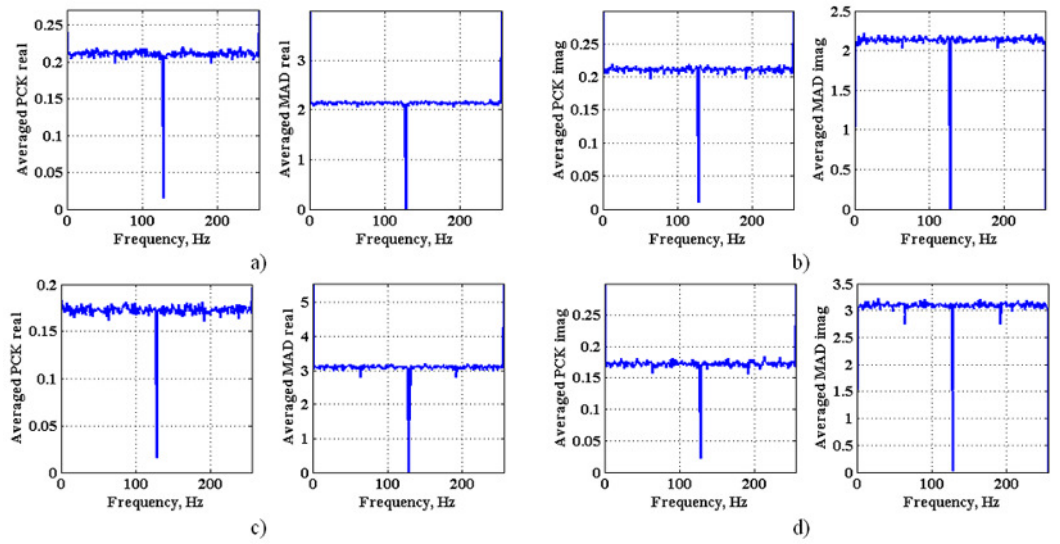

Fig. 11. The plots of $\mathrm{PCK}_{RE}(p)$, $\mathrm{MAD}_{RE}(p)$ (left column) and $\mathrm{PCK}_{IM}(p)$, $\mathrm{MAD}_{IM}(p)$ (right column) for FM signal $s_2(n)$ corrupted by SαS noise with α=1.5 (upper string) and α=1 (bottom string) (γ=4)

a preset threshold ψ) and HL estimator (used otherwise). The recommended value of ψ is about 0.2 (for details see Appendix 1).

The PCK is used also in the censored mean adaptive estimator (CENS) [20]. However, it also exploits a robust estimate of data scale, namely, MAD for a considered data sample. The estimator CENS exploits the facts that the PCK for Gaussian distribution is approximately equal to 0.26 and the standard deviation equals to σ_G=1.483MAD. Then, the formed neighborhood D in case of Gaussian noise approximately corresponds to $3\sigma_G$-neigborhood of the mean (for details see Appendix 1).

In order to understand how distortions are reduced or removed in the CENS-based RDFT-method, let us consider the following example. According to the plots in Fig. 10, the values of MAD are approximately equal to 2, PCK is about 0.25, and than one obtains $D{\approx}9$ (see expression for D in Appendix 1). Taking into account that med$\{R(p,n)\}$ and med$\{I(p,n)\}$ are about 0 (see Fig. 8), the neighborhood limits are from about -9 till about +9. The values belonging to this neighborhood are averaged. Thus, the estimator performs similarly to the sample mean with respect to the values that approximately fit to reasonably narrow limits (see Fig. 8). It can be shown that all values $R(p,n)$ and $I(p,n)$ participate in averaging for the histograms presented in Figs. 3, 5a-d and 8a,b. At the same time, there are outer trimmed values for

the histograms in Figs. 5, 8, i.e., for situations when noise is non-Gaussian and/or intensive. This is desired for a robust estimator to be used in the RDFT framework.

There are also two adaptive myriad estimators (AM1 and AM2) that have been developed recently [38], [39]. The first one estimates γ and α supposing that an underlying distribution is SαS. Estimations of γ and α are based on calculations of MAD and PCK. Then the optimal K is calculated for given estimates $\hat{\alpha}$ and $\hat{\gamma}$ using established dependences [38], [39]. The second adaptive myriad estimator AM2 directly calculates the optimal K using evaluated values of MAD and PCK for the data sample at hand (for details concerning AM1 and AM2 see Appendix 1).

Next, we determine the performance of these estimators. To partly address this problem, consider SαS distributions. There is an approach that allows determining an asymptotic variance of the optimal M-estimator of LP for each distribution from SαS family [41]. Variance of the myriad estimator with optimally set K can be analytically determined as well.

Moreover, it is possible to determine optimal weights for the L-estimator. They are presented in Fig. 12a for data sample of size N=64. For α=2 that corresponds to Gaussian PDF, the sample mean is the optimal L-estimator (all order statistics have the same weights equal to $1/N$). For small α, order statistics with $n \approx N/2$ have considerably larger weights than others, i.e. MED is the quasi-optimal L-estimator. These results serve as good explanations of operation principles for the AATME and CENS estimators.

Now, we analyze the variances of the considered estimators for the LP estimation. They are presented as dependences on α for γ=1 and N=512 in Fig. 12,b. As it can be seen, all adaptive estimators perform well. In the worst cases, variances for them are only 30% larger than for the optimal M-estimator. Adaptive myriad estimators provide the best performance for small α. If the data sample size N decreases, relative performance of all adaptive estimators becomes poorer. The reason is due to the fact that obtained values of the MAD and PCK are less accurate for smaller N.

The main conclusion that follows from this analysis is that the adaptive robust estimators seem to be able to provide improvement if they are used in RDFT framework instead of non-adaptive estimators such as the MED or ATM.

IV. Use of the proposed estimators in RDFT based signal processing

Let us consider the efficiency of the proposed adaptive robust estimators within the RDFT framework of signal processing. Consider MSE of spectral estimates for test signals (TS) $s_1(n)$ and $s_2(n)$ determined by equations (6) and (7).

The following RDFT-methods have been analyzed:

1. Method based on MED estimator ($\dot{X}_{\mathrm{MED}}$);
2. Method based on ATM estimator with fixed β=0.25 ($\dot{X}_{\mathrm{ATM}}$);
3. Method based on WE estimator ($\dot{X}_{\mathrm{WE}}$);
4. Method based on HL estimator ($\dot{X}_{\mathrm{HL}}$);
5. Method based on AATME estimator ($\dot{X}_{\mathrm{AATME}}$);
6. Method based on AD HS estimator ($\dot{X}_{\mathrm{AD\,HS}}$);
7. Method based on CENS estimator ($\dot{X}_{\mathrm{CENS}}$);
8. Method based on adaptive myriad estimator ($\dot{X}_{\mathrm{AM}}$).

The estimators 1-4 are non-adaptive and the estimators 5-8 are adaptive. The estimators 5 and 7 are, in fact, special kinds of adaptive alpha-trimmed mean estimators.

The results of the numerical analysis of the considered methods for harmonic TS $s_1(n)$ corrupted by zero-mean white additive Gaussian noise are summarized in Table 3. Let us start with the analysis of the noise-free case. All non-adaptive estimators introduce certain distortions. However, for the WE and HL estimators these distortions are considerably smaller than for the standard MED. Adaptive estimators except the CENS also introduce distortions. The performance of other adaptive estimators deteriorate, however, they still achieve more accurate results than the MED.

If the input SNR is large enough (consider σ_G=1), the results for the standard DFT and RDFT methods based on the WE and the proposed adaptive estimators are comparable.

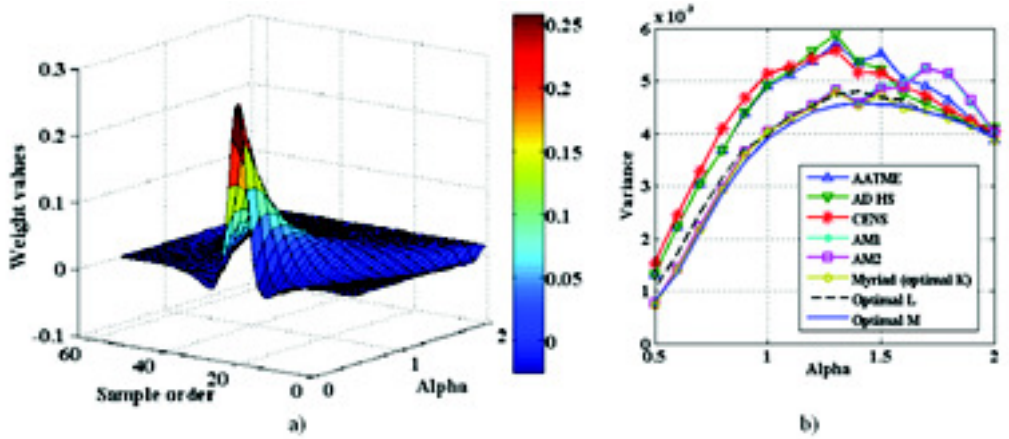

Fig. 12. Optimal weights for L-estimator (N=64) (a) and variance values of LP estimation for the considered adaptive and optimal estimators (N=512) (b) for the SαS processes (γ=1)

For other estimators, the negative effect of introduced distortions is larger than the positive effect of noise suppression.

If the input SNR is small (see data for σ_G=10), MSE values for all robust forms of DFT (except Taguchi's estimator) are smaller than for the standard DFT. The best results are provided by the MED-method; among adaptive estimators the AD HS produces the smallest MSE. Thus, there is no estimator that allows obtaining a minimal MSE for all considered situations. The main advantage of the adaptive robust estimators is that they produce MSE close to minimally reachable for wide ranges of input SNR.

Another set of experiments has been carried out for the FM signal $s_2(n)$ corrupted by heavy-tailed noise. Noise has been simulated as a process with SαS PDF with α from 0.5 till 2 and fixed γ=1. The simulation data are collected in Table 4.

Let us start analysis from Gaussian noise case (α=2). A MED form of DFT produces considerable distortions that result in MSE almost three times larger than for standard DFT. Other RDFT methods provide a smaller MSE, especially the methods based on W, HL and AD HS estimators.

For α=1.5 the influence of heavy-tailed noise on the standard DFT becomes significant. All RDFT forms estimate the signal spectrum more accurately than the standard DFT. Again, the RDFT-methods based on the WE, HL and AD HS estimators provide the best results. Other adaptive estimators have a slightly worse accuracy. The standard DFT fails for noise with Cauchy PDF (α=1). All adaptive methods are almost as accurate as the non-adaptive methods.

Finally, if α=0.5 the standard DFT fails and the MED-method of RDFT achieves the best performance among non-adaptive forms. The best adaptive methods are based on Taguchi's adaptive estimator or CENS in this case. Other adaptive methods perform reasonably well.

Thus, when statistical properties of noise are unknown the main advantage of adaptive estimators used in RDFT framework is that they produce accuracy close to reachable best values.

To demonstrate this advantage, consider two examples. Fig. 13a shows the amplitude spectrum estimate obtained by the standard DFT. As depicted, noise masks the spectrum of the signal and this estimate resembles an estimate of the white noise spectrum. The spectrum estimate obtained by the MED-method of RDFT is demonstrated in Fig. 13b. Here the signal spectrum in the frequency band F=50 Hz is clearly seen but it is distorted (the thin line shows the RDFT spectrum estimate and the thick solid line relates to the true spectrum of FM signal $s_2(n)$). Ampli-

TABLE III
MSE VALUES OF SPECTRUM ESTIMATION FOR TS $s_1(n)$CORRUPTED BY ADDITIVE GAUSSIAN NOISE

σ_G	0	0.5	1	2	4	8	10
$\dot{X}_{\mathrm{ST}}$	0	0.00049	0.00192	0.00782	0.0309	0.249	0.194
$\dot{X}_{\mathrm{MED}}$	0.00545	0.00537	0.00545	0.00613	0.0115	0.0370	0.058
$\dot{X}_{\mathrm{ATM}}$	0.00362	0.00390	0.00478	0.00896	0.0250	0.0862	0.133
$\dot{X}_{\mathrm{WE}}$	0.00058	0.00090	0.00197	0.00626	0.0218	0.0844	0.132
$\dot{X}_{\mathrm{HL}}$	0.00199	0.00211	0.00284	0.00690	0.0237	0.0913	0.142
$\dot{X}_{\mathrm{AATME}}$	0.00498	0.00559	0.00610	0.00864	0.0309	0.1250	0.194
$\dot{X}_{\mathrm{AD\,HS}}$	0.00199	0.00212	0.00285	0.00685	0.0174	0.0592	0.097
$\dot{X}_{\mathrm{CENS}}$	0	0.00051	0.00199	0.00913	0.0301	0.1033	0.156
$\dot{X}_{\mathrm{AM}}$	$8.81{\cdot}10^{-7}$	0.00048	0.00207	0.00809	0.0239	0.0829	0.127

TABLE IV
MSE VALUES OF SPECTRUM ESTIMATION FOR FM SIGNAL $s_2(n)$ CORRUPTED BY NOISE (γ=1)

α	0.5	0.6	0.7	0.8	0.9	1	1.1	1.2
$\dot{X}_{\mathrm{ST}}$	∞	∞	∞	∞	∞	∞	∞	1.11
$\dot{X}_{\mathrm{MED}}$	0.0177	0.0152	0.0133	0.0117	0.0112	0.0102	0.0095	0.0090
$\dot{X}_{\mathrm{ATM}}$	0.0352	0.0270	0.0207	0.0168	0.0143	0.0117	0.0102	0.0088
$\dot{X}_{\mathrm{WE}}$	0.0452	0.0325	0.0236	0.0181	0.0147	0.0114	0.0095	0.0077
$\dot{X}_{\mathrm{HL}}$	0.0504	0.0366	0.0264	0.0204	0.0165	0.0127	0.0105	0.0084
$\dot{X}_{\mathrm{AATME}}$	0.0133	0.0116	0.0111	0.0101	0.0094	0.0089	0.0085	0.0133
$\dot{X}_{\mathrm{AD\,HS}}$	0.0230	0.0197	0.0162	0.0127	0.0104	0.0084	0.0071	0.0230
$\dot{X}_{\mathrm{CENS}}$	0.0179	0.0151	0.0131	0.0111	0.0096	0.0082	0.0073	0.0179
$\dot{X}_{\mathrm{AM}}$	0.0211	0.0182	0.0161	0.0149	0.0121	0.0092	0.0081	0.0211

TABLE V
(TABLE 4 CONTINUED). MSE VALUES OF SPECTRUM ESTIMATION FOR FM SIGNAL $s_2(n)$ CORRUPTED BY SαS PDF (γ=1)

α	1.3	1.4	1.5	1.6	1.7	1.8	1.9	2
$\dot{X}_{\mathrm{ST}}$	0.2929	0.0978	0.36609	0.03078	0.00927	0.00822	0.00797	0.00249
$\dot{X}_{\mathrm{MED}}$	0.0087	0.0080	0.00773	0.00752	0.00726	0.00714	0.00557	0.00653
$\dot{X}_{\mathrm{ATM}}$	0.0077	0.0067	0.00597	0.00550	0.00498	0.00447	0.00660	0.00367
$\dot{X}_{\mathrm{WE}}$	0.0066	0.0053	0.00443	0.00396	0.00338	0.00285	0.00393	0.00209
$\dot{X}_{\mathrm{HL}}$	0.0071	0.0057	0.00472	0.00418	0.00359	0.00300	0.00462	0.00215
$\dot{X}_{\mathrm{AATME}}$	0.0116	0.0077	0.00714	0.00667	0.00616	0.00561	0.00726	0.00481
$\dot{X}_{\mathrm{AD\,HS}}$	0.0197	0.0057	0.00474	0.00420	0.00360	0.00300	0.00462	0.00216
$\dot{X}_{\mathrm{CENS}}$	0.0151	0.0062	0.00535	0.00480	0.00419	0.00361	0.00497	0.00274
$\dot{X}_{\mathrm{AM}}$	0.0182	0.0072	0.00585	0.00502	0.00425	0.00373	0.00493	0.00277

tudes of spectrum estimates for F>50 Hz have sufficiently decreased due to applying the robust estimator. Finally, the adaptive CENS estimator estimates more accurately the signal component spectrum for F=50 Hz (see the plot in Fig. 13c). This simple example demonstrates two advantages of the RDFT methods. First, these methods achieve higher noise suppression in the frequency range where noise-free signal spectrum is practically equal to zero. Second, they also achieve more accurate estimates in the frequency range where the noise-free signal spectrum essentially differs from zero.

Then, if a signal spectrum is estimated based on the RDFT, it becomes possible to carry out denoising with using ideal low-pass filter in spectral domain that has $K(p)$=1 if f_p=f_{upper} and 0 otherwise. Let us set the upper frequency f_{upper} equals to 100 Hz for the considered TS $s_2(n)$. The input signal corrupted by noise with Cauchy PDF and γ=1 is presented in Fig. 14a. The output signal is obtained by the application of RDFT-method based on CENS estimator, ideal low-pass filter and standard inverse DFT. It is shown in Fig. 14b. Obviously, excellent denoising is provided. The impulse noise is removed but also we achieved the suppression of non-impulsive noise components. This can be confirmed by MAE values

$$\mathrm{MAE} = \frac{1}{\mathrm{N}} \sum_{\mathrm{n}=1}^{\mathrm{N}} |\hat{\mathrm{x}}(\mathrm{n}) - \mathrm{x}(\mathrm{n})| \qquad (10)$$

where $\hat{x}(n)$ denotes the reconstructed signal obtained by RDFT filtering approach. MAE=5.505 for the noisy signal shown in Fig. 14a, while for the denoised signal MAE=2.147 without low-pass filtering and MAE=1.417 with low-pass filtering.

V. Conclusions, other related work and perspectives

The general overview of the RDFT-based signal processing approach is presented and the requirements for robust estimators are formulated. Several non-adaptive and adaptive estimators are considered. It has been shown that the main advantage of adaptive estimators is the robustness in wide sense. They also provide a possibility to improve efficiency of signal processing (spectrum estimation, denoising) methods to potentially reachable limits for wide range of noise parameters. In particular, the RDFT based on adaptive estimators can be useful for low input SNRs even if noise is Gaussian. Their application becomes even more practical if noise is non-Gaussian and heavy-tailed. Adaptive estimators CENS and AD HS seem to be the best practical choice. All presented analysis was done for harmonic and FM real-valued signals. However, the same steps are also valid for complex-valued input data.

In this overview, we have concentrated on RDFT applications for spectral analysis and filtering. However, it is worth stressing that the RDFT methods can also be applied in other spectral analysis tasks such as the time-frequency analysis for deriving Wigner-Ville or other distributions [21], [42], estimation of signal parameters [26], etc.

Also note that robust estimators can be useful for data processing based on other than DFT orthogonal transforms as, e.g., discrete cosine transform or Hadamard transforms [27, 43]. Furthermore, the RDFT can be applied to signal subintervals that can be overlapping or not [25]. In this case, data processing becomes similar to the methods used in discrete cosine transform-based denoising [44]. Our future work will concentrate on applying the adaptive robust estimators for processing signals embedded in non-Gaussian noise using other than DFT orthogonal transforms.

Acknowledgement

The work of Igor Djurović is supported in part by the Ministry of Science and Education of Montenegro.

References

[1] H. L. Van Trees, Detection, Estimation and Modulation Theory, CityplaceMcGraw-Hill, StateNew York, 1966.

[2] A. D. Spaulding, D. Middleton, Optimum reception in an impulsive interference environment. Part I: Coherent Detection, IEEE Transactions on Communication, Vol. 25, No. 9, 1977, pp. 910-923.

[3] C. L. Nikias, M. Shao, Signal Processing with Alpha-Stable Distributions and Applications, Wiley, StateplaceNew York, 1995.

Appendix1	
Estimator	Expression
$x(n)$ is the input sample, $n\in[1,N]$; $X^{(q)}$ denotes the q-th order statistic for data sample $x(n)$	
Sample mean	$\hat{X}_{\mathrm{MEAN}}=\sum_{n=1}^{N}x(n)$
Sample median	$\hat{X}_{\mathrm{MED}}=\mathrm{median}\left\{\mathrm{x(n)}\right\}=\begin{cases}X^{([N+1]/2)},\ \text{if N is odd}\\ (X^{(N/2)}+X^{(N/2+1)})/2,\ \text{if N is even}\end{cases}$
Alpha-trimmed mean	$\hat{X}_{\mathrm{ATM}}=\frac{1}{N-N_{\beta1}-N_{\beta2}}\sum_{i=N_{\beta1}+1}^{N-N_{\beta2}}X^{(i)},\ N_{\beta1}{=}N_{\beta2}{=}\beta N,\ 0{=}\beta{=}1$
Wilcoxon estimator	$\hat{X}_{\mathrm{WE}}=\mathrm{median}\left\{\frac{\mathrm{x(1)+x(1)}}{2};\frac{\mathrm{x(1)+x(2)}}{2};...;\frac{\mathrm{x(1)+x(N)}}{2};\frac{\mathrm{x(2)+x(2)}}{2};\frac{x(2)+x(2)}{2};...;\frac{x(N-1)+x(N)}{2};\frac{x(N)+x(N)}{2}\right\}$ median value of the enlarged sample of size $N(N{+}1)/2$
Hodges-Lehmann estimator	$\hat{X}_{\mathrm{HL}}=\mathrm{median}\left\{\mathrm{x(1)};\mathrm{x(2)};...;\mathrm{x(N)};\frac{\mathrm{x(1)+x(N)}}{2};\frac{\mathrm{x(2)+x(N-1)}}{2};...;\frac{x(N/2)+x([N+2]/2)}{2}\right\}$ median value of the enlarged sample of size $N{+}N/2$
Myriad estimator	$\hat{X}_{\mathrm{MYR}}=\mathrm{myriad}\left\{\mathrm{K};\mathrm{x(1)},...,\mathrm{x(N)}\right\}=\arg\min_{\theta\in\Theta}\sum_{\mathrm{n=1}}^{\mathrm{N}}\ln\left\{\mathrm{K}^2+\left[\mathrm{x(n)}-\theta\right]^2\right\}$ where $K{>}0$ denotes the linearization (tuning) parameter
Adaptive Alpha-Trimmed Mean Estimator proposed by A. Taguchi	Alpha-trimmed mean estimator with $N_\beta=[\left\|1-\beta\right\|(N-1)/2]$ where $[\ldots]$ denotes the rounding to the nearest integer value; β is evaluated for each data sample according to the expressions $\beta=\sigma^2/\left(\sigma^2+\sigma_D^2\right),\ \sigma^2=\begin{cases}\sigma_X^2-\sigma_D^2,\ \text{if }\sigma_{\mathrm{X}}^2\geq\sigma_{\mathrm{D}}^2\\ 0,\ \text{otherwise}\end{cases}$, σ_X^2 is the variance of the processing data sample, σ_D^2 denotes the variance of the main distribution (is set a priori)
Adaptive Hard-Switching Estimator	$\hat{X}_{\mathrm{AD\ HS}}=\begin{cases}\hat{X}_{\mathrm{MED}},&K_P\in(0;\psi_0)\\ \hat{X}_{\mathrm{HL}},&K_P\in[\psi_0;+\infty)\end{cases}$, where K_p is an adaptation parameter which uniquely depends on tail heaviness; ψ_0 denotes the threshold value
Adaptive Censoring Estimator	$\hat{X}_{\mathrm{CENS}}=\frac{1}{N}\sum_{n=1}^{N}x(n)\delta(n)$ where $\delta(n)=\begin{cases}1,\ \text{if x(n)}\in[\hat{\mathrm{X}}_{\mathrm{MED}}-\mathrm{D};\ \hat{\mathrm{X}}_{\mathrm{MED}}+\mathrm{D}]\\ 0,\ \text{otherwise}\end{cases}$, $N=\sum_{n=1}^{N}\delta(n)$ $D=4.5\cdot\mathrm{MAD}\cdot\mathrm{PCK}/0.26$
Adaptive Myriad Estimator 1	$\hat{K}_1=\begin{cases}\left(-0.66+0.44e^{1,28\hat{\alpha}}+\ 7.62\cdot10^{-34}e^{39.24\hat{\alpha}}\right)\gamma^{1/\alpha},\ \hat{\alpha}\geq0.3\\ 0,\ \text{otherwise}\end{cases}$ $\hat{\alpha}=1.035\cdot10^3\cdot K_P^4-419.8\cdot K_P^3+55.17\cdot K_P^2+2.051\cdot K_P+0.286$ $\gamma^{1/\alpha}=\mathrm{MAD/C}(\hat{\alpha})$ $C(\alpha)=1.84\alpha^6-14.18\alpha^5+44.36\alpha^4-72.02\alpha^3+64.3\alpha^2-30.3\alpha+7.02$
Adaptive Myriad Estimator 2	$\hat{K}_2=\mathrm{MAD}\cdot\mathrm{f_2\left(K_P\right)}$ $f\left(K_P\right)=3.029\cdot10^5\cdot K_P^6-2.011\cdot10^5\cdot K_P^5+4.95\cdot10^4\cdot K_P^4-5434\cdot K_P^3+265.8\cdot K_P^2+2.36\cdot K_P+0.032$, for $K_P\in(0;0.25]$; $f\left(K_P\right)=2.53\cdot10^5\cdot K_P^2-1.301\cdot10^5\cdot K_P+1.673\cdot10^4$, for $K_P\in(0.25;+\infty]$
Percentile Coefficient of Kurtosis	$\mathrm{PCK}=\mathrm{K_P}=\frac{1}{2}\frac{\mathrm{Q_3-Q_1}}{\mathrm{P_{90}-P_{10}}}$ where Q_1 and Q_3 denote the 1st and the 3rd quartiles, P_{90} and P_{10} are the 90th and 10th percentiles of the processing data sample.
Median Absolute Deviation from Median	$\mathrm{MAD}=\mathrm{median}\left\{\left\|\mathrm{x(n)}-\hat{\mathrm{X}}_{\mathrm{MED}}\right\|\right\}$

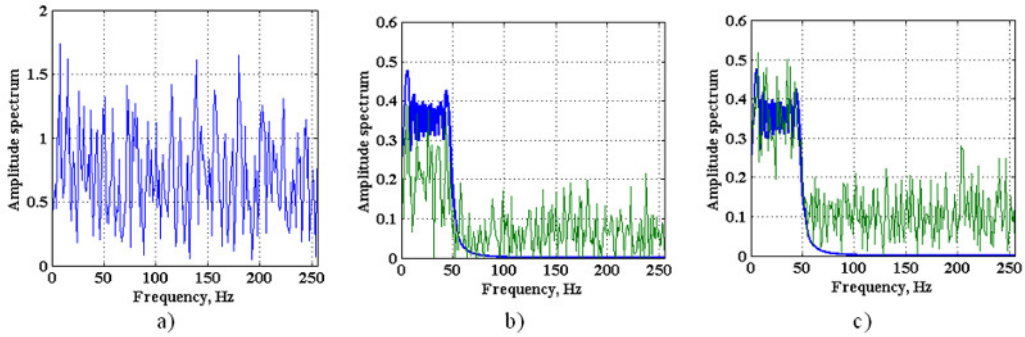

Fig. 13. Amplitude spectrum estimates for FM signal $s_2(n)$ corrupted by noise with Cauchy PDF (γ=1) obtained by the standard DFT (a), MED-method of RDFT (b) and RDFT-method based on CENS (c)

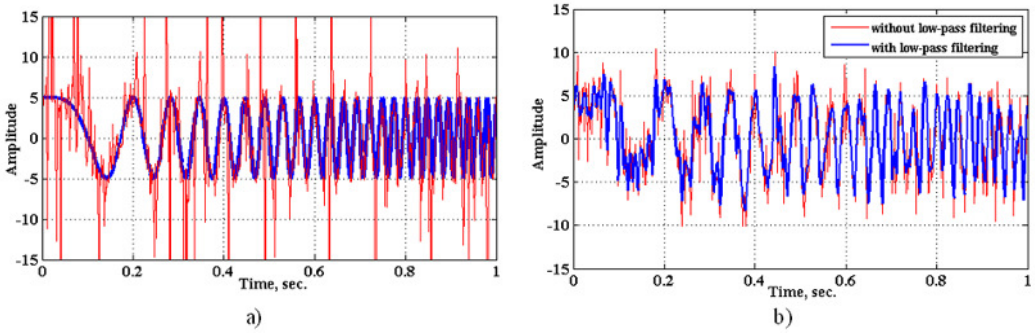

Fig. 14. The TS $s_2(n)$ corrupted by noise with Cauchy PDF (γ=1) (a) and its estimate obtained by RDFT filtering approach based on CENS-method (b)

[4] S. I. Resnick, Heavy Tail Modeling and Teletraffic Data, Annals of Statistic, Vol. 25, No. 5, 1997, pp. 1805-1869.

[5] J. P. Huber, Robust statistics, Wiley, Stateplace-New York, 1981.

[6] J. G. Gonzalez, Robust Techniques for Wireless Communications in Non-Gaussian Environments, Ph.D. Thesis, University of Delaware, Newark, 1997, 169 p.

[7] J. Astola, P. Kuosmanen, Fundamentals of Nonlinear Digital Filtering, CRC Press CityLLC, StateN.Y. CityplaceBoca Raton, 1997.

[8] A.V. Oppemheim, R.W. Schafer, Digital Signal Processing, CityplaceEnglewood Cliffs, NJ, Prentice Hall, 1975.

[9] G. R. Arce, Nonlinear Signal Processing: A Statistical Approach, Wiley, StateplaceNew York, 2005.

[10] J. G. Gonzalez, Statistically-Efficient Filtering in Impulsive Environments: Weighted Myriad Filters, EURASIP Journal on Applied Signal Processing, Vol. 1, 2002, pp. 4-20.

[11] S. Kalluri, G. Arce, Adaptive Weighted Myriad Filter Algorithms for Robust Signal Processing in α-stable Noise Environments, IEEE Transactions on Signal Processing, Vol. 46, No. 2, 1998, pp. 322-334.

[12] I. Shmulevich, G.R. Arce, Spectral design of weighted median filters admitting negative weights, IEEE Signal Processing Letters, Vol. 8, 2001, pp. 313-316.

[13] V. Katkovnik, Robust M-periodogram, IEEE Transactions on Signal Processing, Vol. 46, 1998, pp. 3104-3109.

[14] I. Djurović, V, Katkovnik, LJ. Stanković, Median filter based realizations of the robust time-frequency distributions, Signal Processing, Vol. 81, No 7, 2001, pp. 1771-1776.

[15] I. Djurović, LJ. Stanković, Robust L-estimation based forms of signal transforms and time-frequency representations, IEEE Transactions on Signal Processing, Vol. 51, No. 7, 2003, pp. 1753-1761.

[16] I. Djurović, LJ. Stanković, J.F. Böhme, Myriad Filter Based Form of the DFT, Proceedings of EUSIPCO, France, 2002, 4 p.

[17] I. Djurović, V. Lukin, A. Roenko, Removal of α-stable Noise in Frequency Modulated Signals Using Robust DFT Forms, Telecommunications and Radioengineering, Vol. 61, No 7, 2004, pp. 574-590.

[18] I. Djurović, V. Lukin, Robust DFT with high breakdown point for complex valued impulse noise environment, IEEE Signal Processing Letters, Vol. 13, No 1, 2006, pp. 25-28.

[19] A. Roenko, V. Lukin, I. Djurović, A. Kurekin, A. Zelensky, Filtering of Frequency Modulated Signals Embedded in α-Stable Noise Using Ro-

bust DFT Forms, Proceedings of the International Conference "Modern Problems of Radioengineering, Telecommunications and Computer Science", Lviv-Slavsko, Ukraine, 2006, pp. 228-231.

[20] A. Roenko, V. Lukin, I. Djurovic, LJ. Stankovic, Robust DFT based on adaptive censored estimate for FM signal processing in non-gaussian noise environment, Proceedings of ISSPA, United Arabian Emirates, 2007, 4 p.

[21] I. Djurović, LJ. Stanković, An algorithm for the Wigner distribution based instantaneous frequency estimation in a high noise environment, Signal Processing, Vol. 84, No 3, 2004, pp. 631-643.

[22] I. Djurović, LJ. Stanković, B. Barkat, Robust Time-Frequency Distributions based on the robust Short Time Fourier Transform, Annales des Télécommunications, Vol. 60, No. 5-6, 2005, pp. 681-697.

[23] I. Djurović, Time-Frequency Analysis for SAR and ISAR Imaging, Geospatial Visual Analysis, Springer Netherlands, part 2, 2009, pp. 113-127.

[24] A. Kurekin, D. Marshall, D. Radford, K. Lever, and V. Lukin, Robust Processing of SAR Hologram Data to Mitigate Impulse Noise Impairments, Proceedings of ISIF and IEEE Information Fusion 2005 Conference, Philadelphia, USA, 2005.

[25] I. Djurović, V. Lukin, Robust DFT-based filtering of pulse-like FM signals corrupted by impulsive noise, Signal, Image and Video Processing, Vol. 1, No. 1, 2007, pp. 39-51.

[26] I. Djurović, V. V. Lukin, Estimation of single-tone signal frequency by using the L-DFT, Signal Processing, Vol. 87, No. 6, 2007, pp. 1537-1544.

[27] I. Djurović, LJ. Stanković, J. F. Böhme, Robust L-estimation based forms of signal transforms and time-frequency representations, IEEE Transactions on Signal Processing, Vol. 51, No. 7, 2003, pp.1753-1761.

[28] J. Astola, K. Egiazarian, G. I. Khlopov, S. I. Khomenko, I. V. Kurbatov, V. Ye. Morozov, A. V. Totsky, Application of bispectrum estimation for time-frequency analysis of ground surveillance Doppler radar echo signals, IEEE Transactions on Instrumentation and Measurement, vol. 57, No. 9, 2008, pp. 1949-1957.

[29] R. Suoranta, Amplitude domain approach to digital filtering. Theory and applications of L-filters, Doctor of Technology Thesis, CityplaceEspoo, Technical Research Centre of Finland, 1995, 199 p.

[30] V. V. Lukin, V. P. Melnik, A. B. Pogrebniak, A. A. Zelensky, Techniques and Algorithms of Speckle Noise Reduction for One-Look SAR Images, Proceedings of EUSAR'96, Konigswinter, Germany, 1996, pp. 167-170.

[31] V. V. Lukin, S. K. Abramov, A. A. Zelensky, J. Astola, Blind evaluation of noise variance in images using myriad operation, Proceedings of IS&T/SPIE International Conference on Image Processing: Algorithms and Systems, San Jose, CA, USA, SPIE Vol. 4667, 2002, pp. 192-203.

[32] V. V. Lukin, S. K. Abramov, A. A. Zelensky, J. T. Astola, Use of minimal inter-quantile distance estimation in image processing, Proceedings of SPIE Conference on Mathematics of Data/Image Pattern Recognition, Compression, and Encryption with Applications IX, SPIE Vol. 6315, San Diego, USA, 2006, 12 p.

[33] J. Ilow, D. Hatzinakos, A.N. Venetsanopoulos, Performance of FH SS Radio Networks with Interference Modeled as a Mixture of Gaussian and Alpha-Stable Noise, IEEE Transactions on Communications, 1999, Vol. 20, No. 5, pp. 1-17.

[34] J. L. Hodges, E. L. Lehmann, Estimates of location based on rank tests, Annals of Mathematical Statistics, Vol. 34, No 2, 1963, pp. 598-611.

[35] A. Hoyland, Robustness of the Wilcoxon estimate of location against a certain dependence, The Annals of Mathematical Statistics, Vol. 39, No. 4, 1968, pp. 1196-2001.

[36] V. V. Lukin, S. K. Abramov, N. O. Tulyakova, Dynamic characteristics of some nonlinear 1-D filters, Proceedings of 1999 Finnish Signal Processing Symposium FINSIG'99, Oulu, Finland, 1999, pp. 184-188.

[37] J. G. Gonzalez, G. R. Arce, Optimality of the Myriad Filter in Practical Impulsive-Noise Environments, IEEE Transactions On Signal Processing, Vol. 49, No. 2, 2001, 438-441.

[38] A. Roenko, V. Lukin, I. Djurović, S. Abramov, Adaptation of Sample Myriad Tunable Parameter to Characteristics of SaS Distribution, Proceedings of the Conference on Mathematical Methods in Electromagnetic Theory (MMET 2008), Odessa, Ukraine, 2008, pp. 418-420.

[39] V. Lukin, A. Roenko, S. Abramov, I. Djurović, J. Astola, Bootstrap based adaptation of sample myriad to characteristics of SαS distribution data, Proceedings of IEEE International Symposium on Circuits and Systems, 2009, pp. 1205-1208.

[40] G. Taguchi, Adaptive α-Trimmed Mean Filter with Excellent-Detail Preserving, Proceedings of ICASSP, 1994, pp. 61-64.

[41] H. S. Lim, C. T. Chee, C. H. Teik, On the Optimal Alpha-k Curve of the Sample Myriad, IEEE Signal Processing Letters, Vol. 14, No. 8, 2007, pp. 545-548.

[42] A. Roenko, I. Djurović, V. Lukin, A. Zelensky, Accuracy improvement of the Wigner Distribution estimate in non-gaussian noise environment by means of clipping technique application, Proceedings of the International Conference "Modern Problems of Radioengineering, Telecommunications and Computer Science" (TCSET), Lviv-Slavsko, Ukraine, 2008, pp. 362-365.

[43] I. Djurović, LJ. Stanković, Robust Hadamard transform, Proceedings of the 9th IEEE Mediterranean Conference on Control and Automation, Dubrovnik, Croatia, 2001.

[44] V. V. Lukin, D. V. Fevralev, S. K. Abramov, S. Peltonen, J. Astola, Adaptive DCT-based 1-D filtering of Poisson and mixed Poisson and impulsive noise, CD ROM Proceedings of LNLA, Switzerland, 2008, 8 p.